Tunable nitrogen-doped carbon aerogels as sustainable electrocatalysts in the oxygen reduction reaction

ARTICLE *in* JOURNAL OF MATERIALS CHEMISTRY · MARCH 2013

Impact Factor: 7.44 · DOI: 10.1039/c3ta10352h

4 AUTHORS, INCLUDING:

Tim-Patrick Fellinger
Max Planck Institute of Colloids and Interfa…
39 PUBLICATIONS **946** CITATIONS
SEE PROFILE

Philipp Jäker
ETH Zurich
3 PUBLICATIONS **55** CITATIONS
SEE PROFILE

Journal of Materials Chemistry A

RSC Publishing

PAPER

View Article Online
View Journal | View Issue

Tunable nitrogen-doped carbon aerogels as sustainable electrocatalysts in the oxygen reduction reaction†

Cite this: *J. Mater. Chem. A*, 2013, **1**, 4002

Stephanie-Angelika Wohlgemuth,* Tim-Patrick Fellinger, Philipp Jäker and Markus Antonietti

A one pot hydrothermal synthesis towards nitrogen doped organic aerogels with tunable surface area and nitrogen content is presented. The gels were synthesized from a sustainable glucose carbon precursor with 2-pyrrol-carboxaldehyde (PCA) as the nitrogen source and borax mineral as the structure forming agent. The particle size and hence surface area could be tuned from 75 nm down to 15 nm by varying the amounts of borax added. Similarly, the nitrogen content could be adjusted between 2.0 wt% and 5.5 wt% by varying the amount of PCA added to the glucose solution. Electrochemical testing of the nitrogen doped carbon aerogels as non-metal oxygen reduction catalysts revealed increasing activity with higher surface area and higher nitrogen content, as well as excellent long term stability. Our work thereby demonstrates the high potential of hydrothermal carbon materials and also provides a facile approach toward tunable nitrogen doped aerogels which should be useful for a wide range of applications.

Received 23rd January 2013
Accepted 24th January 2013

DOI: 10.1039/c3ta10352h

www.rsc.org/MaterialsA

Introduction

Aerogels are a class of materials with defined nano-architectures that find applications in thermal and acoustic insulation, sorption, catalysis, and chromatography and as electrode materials.[1–3] In simple terms, they are gels in which the liquid component has been replaced by air. They are consequently extremely lightweight materials containing many voids within a continuous solid matrix which allows for excellent mass transport and good thermal insulation.[1,4] Inorganic aerogels have been prepared from various materials such as metal oxides or chalcogenides.[3,5,6] The first organic aerogels were introduced by Pekala *et al.* in 1989 and synthesized by the condensation of resorcinol-formaldehyde (RF) using acid or base catalysts. These resulting "organic aerogels" contain abundant oxygen functionalities and may be converted into high carbon content "carbon aerogels" *via* pyrolysis, which usually results in higher electrical conductivity and therefore opens the door for electronic applications.[2,7] Carbon aerogels have been used as supports for noble[8–11] as well as non-noble metal[12,13] catalysts in the oxygen reduction reaction. In 2009, Gong *et al.* reported the first efficient metal-free catalyst for the oxygen reduction reaction, based on nitrogen-doped carbon nanotube arrays.[14] Since then efforts have been increasing to find metal-free alternatives to conventional platinum catalysts, for which heteroatom doped carbon materials have proven to be high potential candidates.[14–21] Most examples involve nitrogen doped carbon materials, but boron[20] as well as sulfur[19,21,22] have also been reported to enhance electrocatalytic activity of the material. Jin *et al.* reported on RF-based nitrogen-doped xerogels synthesized using ammonia as the nitrogen source and cobalt nitrate as catalyst. The xerogels exhibited high ORR electrocatalytic activity and good stability in acidic media.[23]

Nitrogen doped aerogels have been prepared by slight modifications of the RF system, *e.g.* using melamine-formaldehyde.[24,25] One of the main drawbacks of these synthesis approaches however is the multi-step synthesis procedure that can last up to several days and the usually fossil based nature of the precursors.

Hydrothermal carbonization (HTC) may briefly be described as a mimic of natural coalification on a timescale of hours and days rather than millions of years. The biggest advantage of HTC is the possibility to use cheap and readily available precursors such as biowaste or simple carbohydrates for the synthesis of valuable carbon materials.[26,27] HTC has been exploited to synthesize organic aerogels using the albumin directed hydrothermal carbonization of glucose which gave rise to inherently nitrogen doped aerogels, although tuning of the nitrogen content or surface area was not possible.[28] These aerogels showed only moderate electrocatalytic activity in the oxygen reduction reaction under alkaline conditions.[22] A second hydrothermal approach is the borax-catalyzed hydrothermal carbonization of glucose. The advantage of this approach is that the particle size and therefore the surface area of the aerogel

Max Planck Institute of Colloids and Interfaces, Am Mühlenberg 1, 14467 Potsdam, Germany. E-mail: stephanie.wohlgemuth@mpikg.mpg.de; Fax: +49-331-56-9502; Tel: +49-331-567-9562

† Electronic supplementary information (ESI) available. See DOI: 10.1039/c3ta10352h

may be adjusted (similar to the RF system) by varying the amount of borax added.[29] So far, heteroatom doping of these aerogels has not been reported, which would be favorable to broaden their range of applications. Therefore, we herein present the extension of the borax-mediated hydrothermal carbonization of glucose towards the incorporation of nitrogen to synthesize nitrogen doped carbon aerogels. We show that the electrocatalytic performance of the nitrogen doped carbon aerogels in the oxygen reduction reaction can be significantly enhanced by adjusting parameters such as nitrogen content and surface area.

Results and discussion

In the borax-mediated aerogel formation from glucose, the particle size and hence surface area may be controlled by the amount of borax added to the initial reaction mixture. The more borax is added, the smaller the particles and hence the higher the surface area. A proposed mechanistic explanation is given elsewhere.[29] Briefly, borax is assumed to increase the overall reactivity between HTC intermediates due to a secondary catalytic effect. According to the LaMer model, this accelerated reaction rate rapidly results in a critical supersaturation and hence a nucleation burst.[30] The large number of seeds results in smaller particles in the growth phase. These particles eventually give rise to the aerogel morphology by aggregation and covalent crosslinking amongst each other.

For the herein presented nitrogen-doped aerogels, it was investigated whether the introduction of a dopant influences this behavior. 2-Pyrrol-carboxaldehyde (PCA) was used as the nitrogen source and simply added to a glucose–borax solution. Three nitrogen doped organic aerogels were synthesized, each from a reaction mixture containing 0.8 g PCA, 6.0 g glucose and 14.0 g water. The borax amount was varied from 150 mg (label **B1**) to 300 mg (label **B2**) and 600 mg (label **B3**). The resulting aerogels were labeled **N1B1**, **N1B2** and **N1B3** in order of increasing borax addition. The group of these three samples is hereafter referred to as the borax series.

It was further investigated whether the nitrogen content of the doped aerogels could be tuned by varying the concentration of PCA added to the system. In addition to the initial experiments which contained 0.8 g of PCA (label **N1**) in the reactant mixture, another two samples with higher amounts of PCA (1.3 g, label **N2** and 2.0 g, label **N3**) were synthesized. All other parameters were kept constant. Each solution contained 300 mg of borax. The resulting aerogels were labeled **N1B2**, **N2B2** and **N3B2** in order of increasing PCA addition. The group of these three samples is hereafter referred to as the PCA series.

Morphology, chemical composition and textural properties of the organic aerogels

Transmission electron microscopy (TEM) images (Fig. 1) show the typical borax-mediated aerogel morphology that was already observed by Fellinger *et al.*,[29] *i.e.* a matrix comprising interconnected particles. The borax series is shown in the first row (Fig. 1a–c), nicely demonstrating the decrease in particle size with increasing borax addition. The particle size decreases from an average diameter of 75 nm, to 23 nm and finally to 16 nm with increasing borax addition. The PCA series is shown in Fig. 1b, d and e in the order of increasing nitrogen content. Between N1B2 and **N2B2**, there is no notable particle size difference. The average particle diameters determined from TEM observations are 23 nm in both cases (Fig. 1b and d). It seems that within this PCA concentration range, borax is the size determining factor and PCA addition does not interfere with the particle morphology. At the very high PCA levels in **N3B2** (1 : 3 weight ratio of PCA to glucose, Fig. 1e) the average particle size increases to 30 nm, presumably because at such high PCA amounts, some of the borax is scavenged by the nitrogen source, thus lowering the "effective borax amount interacting with glucose".

The elemental composition and textural properties determined by nitrogen sorption of the organic aerogels are summarized in Table 1. Within the borax series the nitrogen contents are similar, varying between 2.0 wt% and 2.2 wt%. As seen from the TEM images, the surface area increases with increasing borax addition and the resultant decrease in particle size. Within the PCA series the nitrogen content increases with increasing PCA addition, ranging from 2.0 wt% to 5.5 wt%. In accordance with TEM data, the surface areas of **N1B2** and **N2B2** are within a similar range while the surface area of **N3B2** drops down to 80 $m^2\ g^{-1}$ due to the observed increase in size.

The loss of surface area in **N3B2** could make the increased nitrogen doping levels trivial when it comes to electrochemical applications, where high surface areas and good mass transport are crucial. We therefore synthesized an additional nitrogen doped aerogel, whereby the highest PCA (2.0 g, label **N3**) and the highest borax amount (600 mg, label **B3**) were combined. The sample **N3B3** exhibited the desired properties, *i.e.* both high nitrogen content (5.4 wt%) and high surface area (366 $m^2\ g^{-1}$) with an average particle diameter of 15 nm (Table 1 and Fig. 1f). These results nicely demonstrate that using our synthesis method, both the surface area and nitrogen content can be tuned individually depending on the amount of borax or nitrogen source added.

All nitrogen doped organic aerogels after HTC at 180 °C exhibit Type IV/H3 reversible sorption isotherms with limited hysteresis loops (Fig. 2a and b).[28] The lack of an adsorption plateau at high relative pressures as well as the broad pore size distribution for all samples are indicative of slit shaped pores in an open pore system (Fig. 2e). The increase in the adsorbed volume at p/p_0 near unity is attributed to capillary condensation in large mesopores or small macropores,[28] the presence of which should be beneficial for efficient mass transport of electrolyte and oxygen during the electrocatalytic reactions.

Representative XPS data of **N3B3** shows that the vast majority (94.3%) of the nitrogen contents derives from pyrrolic nitrogen (Table 2 and Fig. S1a and b†).[27] Also, the nitrogen contents derived from XPS (*i.e.* surface sensitive) and from elemental analysis (bulk) are very similar (5.8 at % and 5.4 wt%, respectively (Table 1)), indicating a homogeneous nitrogen distribution between the particle core and surface.

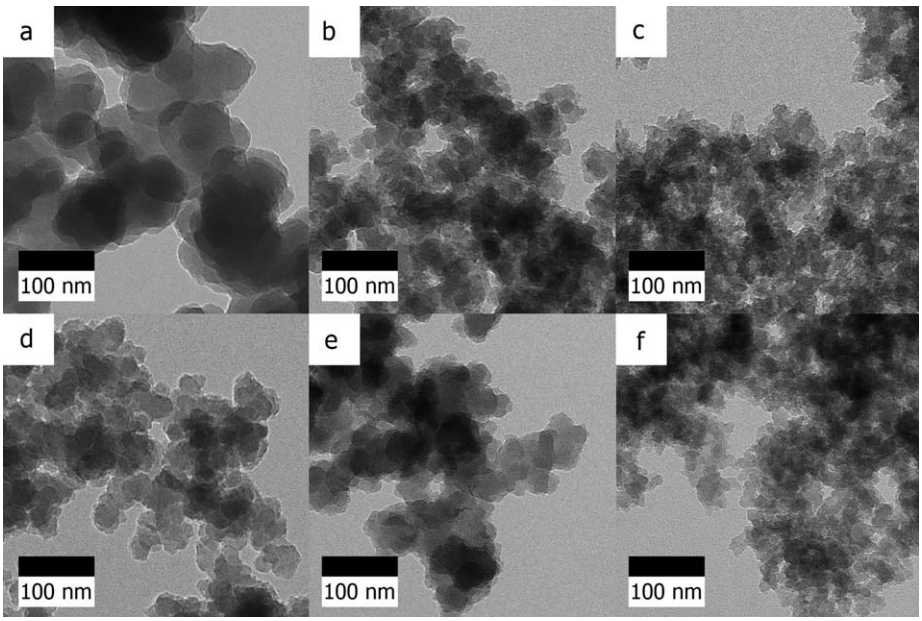

Fig. 1 TEM images of (a) **N1B1**, (b) **N1B2**, (c) **N1B3**, (d) **N2B2**, (e) **N3B2** and (f) **N3B3**.

Fourier-transform infrared spectroscopy (FT-IR) of the PCA series was used to investigate the effect of increasing nitrogen concentration on the surface functionalities of the material (Fig. 3). A spectrum of **B2**, *i.e.* an undoped organic aerogel (synthesized from glucose and 300 mg borax), is shown for reference. The broad band at ~3500 cm^{-1} to ~3300 cm^{-1} is due to the presence of abundant hydroxyl groups in the hydrothermal carbon. Other bands that are typical for glucose-derived hydrothermal carbon are seen at ~2900 cm^{-1} and at ~1010 cm^{-1} and are attributed to aliphatic methyl/methylene and furanic C=C–O vibrations, respectively. These bands are similar in both undoped and nitrogen doped aerogels and are hence not discussed further. Regions with notable differences are highlighted in grey. The band at ~1710 cm^{-1} corresponds to carbonyl (aldehyde, ketone, carboxylic acid) functionalities whereas the bands at ~1620 cm^{-1} and ~870 cm^{-1} are attributed to aromatic C=C and C=***C–H*** vibrations, respectively. With increasing nitrogen content, the intensity of the aromatic C=C and C=C–H bands relative to the carbonyl band increases, indicating a more aromatic carbon framework. Notably, aromatic, cyclic C=N bonds also give rise to bands in the ~1620 cm^{-1} region. From XPS data it is known that 94.3% of surface nitrogen is bound as pyrrol, so it was concluded that the increased number of pyrrolic units in the hydrothermal

Table 1 Elemental composition and textural properties of heteroatom doped carbon aerogels before and after pyrolysis at 900 °C. The specific conductivity values are shown on the right

	Elemental composition by EA (wt%)/XPS (at %)				Textural properties					
Sample	C	H	N	O*	S_{BET} m^2 g^{-1}	V_{total} cm^3 g^{-1}	V_{meso} cm^3 g^{-1}	V_{micro} cm^3 g^{-1}	D_{av} nm[a]	σ S m^{-1}
N1B1	64.2	4.4	2.2	29.3	42	0.07	0.07	0.00	75	—
N1B2	53.8	4.0	2.0	40.3	192	0.32	0.27	0.05	23	—
N1B3	57.5	4.2	2.2	36.1	427	0.71	0.60	0.11	16	—
N2B2	64.2	4.8	4.1	27.0	149	0.28	0.25	0.03	23	—
N3B2	64.8	4.6	5.5	25.1	80	0.17	0.15	0.02	30	—
N3B3	62.4/78.7	4.6	5.4/5.8	26.8/15.5	366	0.44	0.33	0.11	15	—
N1B1_900	90.8	0.9	3.2	5.1	28	0.09	0.09	0.00	74	925
N1B2_900	86.6	1.0	3.0	9.4	179	0.36	0.32	0.04	17	549
N1B3_900	90.5	0.4	3.5	5.6	305	0.43	0.34	0.09	15	406
N2B2_900	88.9	1.0	4.6	5.6	159	0.33	0.29	0.04	22	588
N3B2_900	88.8	0.2	5.9	5.1	105	0.19	0.16	0.03	24	490
N3B3_900	88.4/92.4	1.3	6.3/4.5	3.3/3.1	265	0.48	0.41	0.07	11	433
B2_900	93.0	1.5	—	2.9	373	0.40	0.27	0.13	16	641

[a] D_{av} = average diameter of aerogel particles determined from TEM images, σ = specific conductivity as determined by impedance spectroscopy, * = oxygen values from elemental analysis are calculated from the rest mass of C, N, H and S analysis.

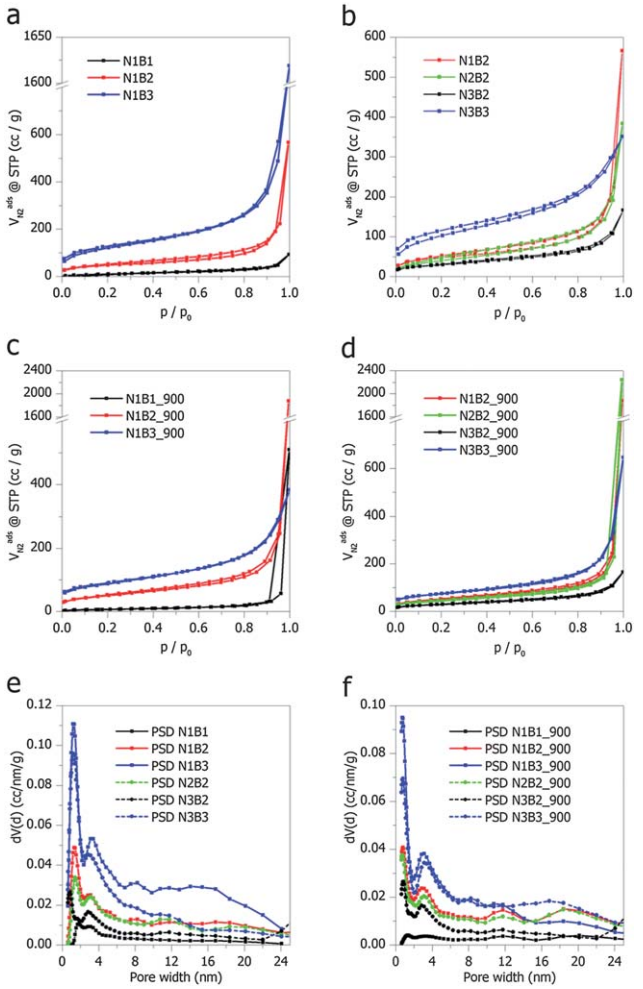

Fig. 2 Nitrogen sorption isotherms of (a) borax series after HTC at 180 °C and (b) PCA series and **N3B3** after HTC at 180 °C, (c) borax series after pyrolysis at 900 °C, (d) PCA series and **N3B3** after pyrolysis at 900 °C. Pore size distributions (QSDFT model) obtained for (e) as-synthesized aerogels after HTC at 180 °C and (f) carbon aerogels after pyrolysis at 900 °C.

Table 2 Peak assignments for the C1(s) and N1(s) photoelectron envelopes for samples **N3B3** and **N3B3_900**

	Binding energy (eV)/fraction of species (%)		
Peak	**N3B3**	**N3B3_900**	Assignment
C1s	285.0/73.0	285.0/65.3	C1 sp^2 C–C or C–H[21,31,32]
	286.7/16.4	286.2/16.0	C2 C–O/C–N/C–S[21]
	288.5/7.1	287.4/8.7	C3 C═O/C═N[21,33]
	—/—	289.0/5.9	C4 O═C–O[34]
	291.0/3.6	291.4/4.2	C5 π–π* shake up satellite[32,35]
N1s	398.1/5.7	398.7/33.5	N1 pyridinic[27,32]
	400.2/94.3	—/—	N2 pyrrolic[27]
	—/—	401.2/54.29	N3 quaternary[21,27]
	—/—	403.7/12.3	N4 pyridinic N–oxide[21]

carbon framework results in the increased aromaticity as seen by FT-IR analysis. The overall data lead us to the assumption that the pyrrol unit in the PCA precursor is incorporated into the hydrothermal carbon framework mainly by aldol or

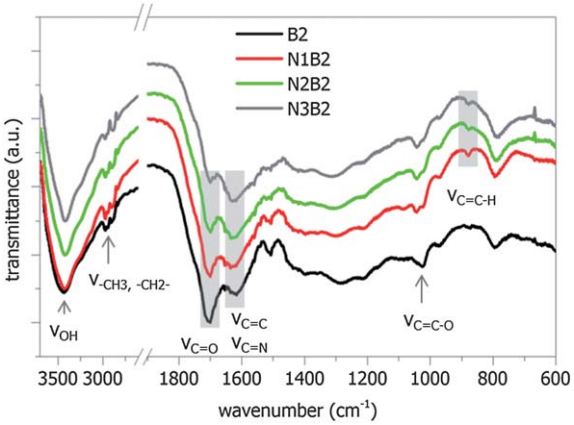

Fig. 3 FT-IR spectra of the PCA series. A spectrum of **B2** (*i.e.* an undoped organic aerogel) is shown for reference (black line). The spectra were vertically shifted from their original position for clarity.

electrophilic aromatic substitution (EAS) mechanisms. Note that while the five membered ring in PCA is initially deactivated with respect to EAS, it becomes activated if the aldehyde functionality reacts first, *e.g.* through an aldol reaction or to form an acetal with alcohol functionalities of glucose or on the condensed hydrothermal framework. Aromatic nitrogen containing precursors therefore are assumed to react differently with glucose during HTC compared to other commonly used nitrogen sources such as amino acids or aminated sugars. In those cases, Maillard type reactions have been proposed which result in a variety of nitrogen species (amine, pyrrol, pyrazine, *etc.*) in the final hydrothermal product.[36]

Conversion of organic aerogels to carbon aerogels *via* pyrolysis

The aerogels obtained after HTC at 180 °C contain between 53 wt% and 65 wt% carbon and can therefore be classified as "organic" aerogels. In order to obtain "carbon" aerogels with an increased conductivity and material stability, pyrolysis at 900 °C was carried out. Table 1 summarizes the elemental compositions and textural properties of the pyrolized carbon aerogels. The carbon aerogels contain around 90 wt% carbon and have retained similar heteroatom contents. The slight increases are simply due to the relative changes in weight after loss of oxygen and hydrogen containing functionalities. The last column shows the corresponding specific conductivity values, confirming that pyrolysis has rendered the aerogels conducting.

TEM and SEM analyses show retention and homogeneity of the aerogel morphology (Fig. S2 and S3,† respectively) in all cases. The particle size has decreased slightly for most samples which is expected to arise from further condensation and carbonization of the carbonaceous framework. X-ray diffractograms of a representative sample (**N2B2_900**) show two broad peaks at around 22° and 43°, which correspond to the (002) and (100) reflections of graphite, respectively (Fig. S4†).[37] The large shift towards smaller angles indicates a large interlayer spacing. This is typical for hydrothermal carbon, and the interlayer

spacing is expected to increase further due to the presence of dopants, because they can induce packing defects. Comparing the diffractogram of a nitrogen doped carbon aerogel with that of an undoped carbon aerogel (**B2_900**) however does not show a notable difference in the (002) peak position.

High resolution transmission electron microscopy (HRTEM) images show that both the undoped (Fig. S5a†) and nitrogen doped carbon aerogels (represented by **N3B3_900**, Fig. S5b†) have highly disordered graphitic layers.

All carbon aerogels continue to exhibit type IV/H3 nitrogen sorption isotherms (Fig. 2c, d and f). The decrease in the apparent BET surface areas for most of the samples is due to (a) overall contraction of the carbon framework upon further carbonization and (b) micropore shrinkage which results in ultramicropores (*i.e.* <1 nm) which cannot be detected by nitrogen sorption.[38] The overall order of the surface area between the samples is however similar to that observed for the as-synthesized organic aerogels.

Electrochemical characterization of carbon aerogels

The nitrogen doped carbon aerogels pyrolized at 900 °C were tested for their ORR related electrocatalytic activity. Three main points were investigated: (1) the effect of surface area of the nitrogen doped carbon aerogels, *i.e.* a comparison among the borax series. (2) The effect of the nitrogen content of the nitrogen doped carbon aerogels, *i.e.* a comparison among the PCA series. (3) The electrocatalytic performance of **N3B3_900**, *i.e.* high nitrogen content and high surface area.

Powder composite electrodes were prepared by depositing inks made from ground monoliths using Nafion as a binder onto glassy carbon electrodes (see ESI for detailed experimental methods†). Cyclic voltammetry (CV) and linear sweep voltammetry (LSV) using a rotating disk electrode (RDE) were carried out in 0.1 M KOH. Featureless voltammetric curves were observed for all samples in an N_2-saturated solution. A strong cathodic peak is seen upon saturating the solution with O_2, showing the catalytic effect of the nitrogen-doped borax gels towards oxygen reduction (Fig. 4a and b).

Analysis of the polarization curves for borax concentration series (Fig. 4c) reveals a direct correlation of surface area, onset potential and maximum current density. The higher the surface area (*i.e.* the more borax is added), the better the onset potential and maximum current densities over the scanned potential range. Notably, the low surface area of **N1B1_900** (28 m^2 g^{-1}) results in a poor catalyst performance which is even lower than pure Vulcan carbon (dashed black line). **N1B2_900** exhibits only slightly improved current densities, but a similar onset potential, to an undoped aerogel containing the same amount of glucose and borax, but no PCA (**B2_900**, red dashed line). It is assumed that the nitrogen content of 3.0 wt% improves material conductivity, but otherwise has no obvious effect on the electrocatalytic performance.

Analysis of the polarization curves for PCA concentration series (Fig. 4d) shows that the overall catalytic performance is in the order **N3B2_900** < **N1B2_900** < **N2B2_900**, *i.e.* the sample with the highest nitrogen doping levels has the lowest

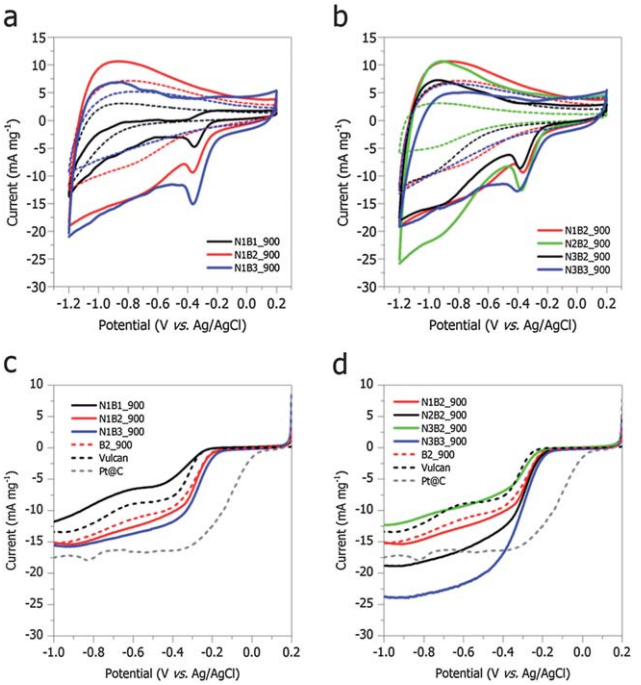

Fig. 4 Cyclic voltammograms obtained in N_2-saturated (dashed lines) and O_2-saturated (solid lines) 0.1 M KOH for (a) borax concentration series, (b) PCA concentration series and **N3B3_900**. Polarization curves obtained with an RDE in 0.1 M KOH at 1600 rpm for (c) borax concentration series, (d) PCA concentration series and **N3B3_900**. Data for undoped **B2_900** (dashed red line), Vulcan XC 72R (dashed black line) and 20 wt% Pt@C (dashed grey line) are shown for reference.

electrocatalytic activity. This is most likely due to the decreased surface area of **N3B2_900** compared to the other two samples. As expected, the drop in surface area due to the increased particle size counteracts the potential benefits of higher nitrogen contents. **N3B2_900** has a similar activity to Vulcan carbon whereas **N2B2_900** is already more comparable to Pt@C. Between **N1B2_900** and **N2B2_900**, the onset potential is similar but the current density varies, further supporting the earlier statement that nitrogen doping improves conductivity but has otherwise no effect.

N3B3_900 which has both high nitrogen content and surface area very clearly exhibits the best overall catalytic performance out of all tested samples (Fig. 4e). The current densities now exceed even those of Pt@C and the onset potential is slightly improved compared to the remaining carbon aerogels. We attribute this increase in performance to an increased number of active sites on the carbon material surface.

Since sample **N3B3_900** exhibited the best performance in terms of current density and onset potential, further analysis was carried out to investigate the long term stability of the material, methanol tolerance and electron transfer number. Chronoamperometric data (Fig. 5a) indicate that the carbon aerogel is very stable under the tested conditions (0.1 M KOH, $V = -0.5$ V *vs.* Ag/AgCl), retaining >85% of its initial current density after 200 min (blue line). Comparatively, the platinum catalyst current density drops down to 75% (grey dashed line).

To investigate possible methanol crossover effects, 2 ml of methanol were injected during chronoamperometry at the

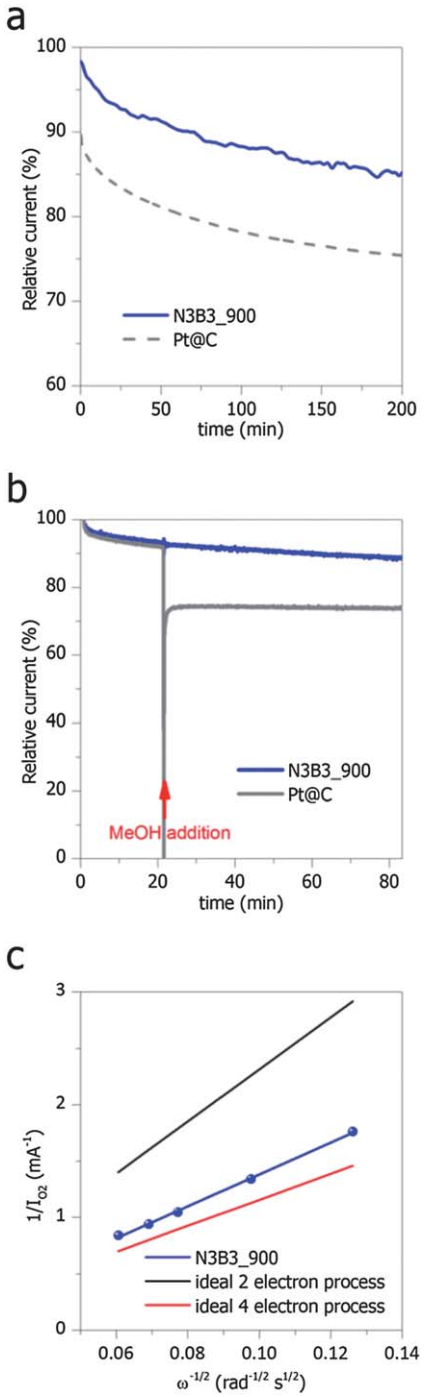

Fig. 5 Data for **N3B3_900**. (a) Chronoamperometry, (b) methanol crossover and (c) the Koutecky–Levich plot of **N3B3_900** in comparison with an ideal 2 electron process (black line) and an ideal 4 electron process (red line).

point indicated by the red arrow in Fig. 5b. The data clearly show that while the commercial platinum catalyst is poisoned after methanol addition, **N3B3_900** is virtually unaffected. The nitrogen doped carbon catalyst therefore exhibits excellent methanol tolerance which is a widely recognized advantage of nitrogen-doped materials and has previously been observed by other groups.[14,16] Koutecky–Levich analysis was used to determine the electron transfer number at $V = -0.5$ V *vs.* Ag/AgCl for **N3B3_900**. Fig. 5c shows the linear Koutecky–Levich plot of **N3B3_900** in comparison with an ideal 2 electron process and an ideal 4 electron process. The slope of **N3B3_900** is evidently more similar to that of an ideal 4 electron process and yields an electron transfer number of 3.3 at −0.5 V *vs.* Ag/AgCl. 4 electron processes are favorable for fuel cell applications because the alternative 2 electron process produces H_2O_2 as an intermediate which may poison the catalyst.[39]

It has previously been suggested that certain binding states of nitrogen are favorable for promoting catalytic behavior of the carbon material in the oxygen reduction reaction. However, DFT calculations suggest that nitrogen is not itself the catalytically active site, but that the high electronegativity of nitrogen polarizes the C–N bond, and the adjacent carbon atom therefore has a reduced energy barrier towards ORR.[23,40] Matter *et al.* suggested pyridinic edge sites as likely active sites because edge planes facilitate oxygen chemisorption.[41] Luo *et al.* synthesized purely pyridinic nitrogen doped carbons and found them to be selective for a 2 electron reduction pathway.[42] Liu *et al.* recently proposed that graphitic nitrogen accounts for good catalytic activity, though in their case the nitrogen content did not directly correlate with the catalyst performance – materials (nitrogen-doped mesoporous graphitic arrays) with higher nitrogen content showed lower selectivity and activity.[18] In yet another report, Strelko *et al.* suggested that pyrrolic nitrogen should give rise to the best electron transfer capabilities.[43] XPS analysis of **N3B3_900** reveals that the relative proportions of pyridinic and graphitic nitrogen species are 33.5% and 54.29%, respectively. No pyrrolic species could be detected in the pyrolized sample, while 12.3% of the nitrogen was present as pyridinic N–oxide (Table 2 and Fig. S1 day†). Overall, the XPS analysis did not yield conclusive results as to which nitrogen species could be responsible for the high catalytic behavior of **N3B3_900**. It is possible that pyridinic and graphitic nitrogen sites promote different selectivities (*i.e.* 2 or 4 electron), giving rise to the observed electron transfer number of 3.3.

Finally, it could be argued that the high performance of the nitrogen doped carbon catalyst could be due to trace metals, arising from residual borax or from impurities in the glucose precursor. We therefore carried out inductively coupled plasma atomic emission spectroscopy (ICP OES) on **N3B3_900**. The only metal that could be found was iron at a very low concentration of 0.0035 wt% (*i.e.* 35 ppm). Also note that the XPS survey scans of **N3B3** and **N3B3_900** do not exhibit any peaks other than those corresponding to C, O or N (Fig. S6†). We are therefore confident that the performance of our catalyst is due to the high nitrogen content and surface area only, given that the amount of trace metals is negligible. Even though results are promising so far, our glucose based nitrogen doped aerogels are still behind previously reported nitrogen doped carbon materials in terms of overall catalytic performance.[14,18,23] However, it should be noted that our system is based mainly on a cheap, sustainable carbohydrate precursor while previous systems have been based on resorcinol-formaldehyde,[23] carbon nanotubes,[14] or organic dyestuff in combination with silica templates.[18] The herein presented results

should therefore also be taken into consideration in the context of sustainability and the possibilities that hydrothermal carbonization have to offer.

Conclusion

Using a modification of the borax-mediated aerogel formation in the hydrothermal carbonization of glucose it was possible to successfully introduce nitrogen as a dopant. 2-Pyrrol-carboxaldehyde (PCA) was thereby simply added to a borax–glucose solution and hydrothermally treated at 180 °C. Supercritical CO_2 drying was used to prevent collapse of the nanostructured aerogels due to capillary forces. It was shown that both the particle size (and hence surface area) and the nitrogen content can be tuned by varying the amounts of borax or PCA used. Pyrolysis at 900 °C of the organic aerogels rendered the resulting carbon aerogels electrically conducting. Electrochemical testing of the carbon aerogels as catalysts in the oxygen reduction reaction showed that catalytic activity increases with higher surface area and with higher nitrogen content. A carbon aerogel with high surface area and high nitrogen content was engineered to maximize catalytic performance. The obtained sample **N3B3_900** exhibited drastically improved current densities compared to a platinum catalyst (but lower onset potential), as well as excellent long term stability. Koutecky–Levich analysis indicated that the selectivity of **N3B3_900** tended towards an ideal 4-electron process. Importantly, the first carbohydrate-derived, non-metal electrocatalyst, synthesized *via* a sustainable hydrothermal carbonization (HTC) technique, to partially outperform noble platinum catalysts was presented. This work therefore demonstrates the powerful potential of HTC derived materials for energy-related applications and how they can contribute to future clean energy solutions. Experiments of combining the high potential of our glucose-derived aerogels with more efficient metal catalysts are currently ongoing in our laboratory and will be presented in a future publication.

Acknowledgements

The authors would like to acknowledge Dr. Magdalena Titirici and Dr. Robin White for scientific discussions. Sylvia Pirok, Heike Runge and Rona Pitschke are acknowledged for elemental analysis and SEM measurements. XPS analysis was carried out by Carmen Serra at the University of Vigo, Spain. HRTEM measurements were carried out by Sören Selve at the TU Berlin. ICP-OES measurements were carried out at the university of Potsdam.

References

1 A. C. Pierre and G. M. Pajonk, *Chem. Rev.*, 2002, **102**, 4243–4266.
2 J. Biener, M. Stadermann, M. Suss, M. A. Worsley, M. M. Biener, K. A. Rose and T. F. Baumann, *Energy Environ. Sci.*, 2011, **4**, 656–667.
3 G. M. Pajonk, *Appl. Catal.*, 1991, **72**, 217–266.
4 J. Fricke and T. Tillotson, *Thin Solid Films*, 1997, **297**, 212–223.
5 J. L. Mohanan, I. U. Arachchige and S. L. Brock, *Science*, 2005, **307**, 397–400.
6 S. S. Kistler, *Nature*, 1931, **127**, 741.
7 R. W. Pekala, *J. Mater. Sci.*, 1989, **24**, 3221–3227.
8 W. S. Baker, J. W. Long, R. M. Stroud and D. R. Rolison, *J. Non-Cryst. Solids*, 2004, **350**, 80–87.
9 E. Guilminot, F. Fischer, M. Chatenet, A. Rigacci, S. Berthon-Fabry, P. Achard and E. Chainet, *J. Power Sources*, 2007, **166**, 104–111.
10 N. Job, F. Maillard, J. Marie, S. Berthon-Fabry, J.-P. Pirard and M. Chatenet, *J. Mater. Sci.*, 2009, **44**, 6591–6600.
11 J. Marie, S. Berthon-Fabry, M. Chatenet, E. Chainet, R. Pirard, N. Cornet and P. Achard, *J. Appl. Electrochem.*, 2007, **37**, 147–153.
12 S. Y. Ye and A. Vijh, *J. Solid State Electrochem.*, 2005, **9**, 146–153.
13 S. Y. Ye and A. K. Vijh, *Int. J. Hydrogen Energy*, 2005, **30**, 1011–1015.
14 K. P. Gong, F. Du, Z. H. Xia, M. Durstock and L. M. Dai, *Science*, 2009, **323**, 760–764.
15 G. Liu, X. Li, J.-W. Lee and B. N. Popov, *Catal. Sci. Technol.*, 2011, **1**, 207–217.
16 L. T. Qu, Y. Liu, J. B. Baek and L. M. Dai, *ACS Nano*, 2010, **4**, 1321–1326.
17 Z. Yang, Z. Yao, H. Nie, X. Zhou, Z. Liu and S. Huang, *Chem. Commun.*, 2011, **48**, 1027–1029.
18 R. L. Liu, D. Q. Wu, X. L. Feng and K. Mullen, *Angew. Chem.,Int. Ed.*, 2010, **49**, 2565–2569.
19 Z. Yang, Z. Yao, G. Li, G. Fang, H. Nie, Z. Liu, X. Zhou, X. a. Chen and S. Huang, *ACS Nano*, 2011, **6**, 205–211.
20 L. Yang, S. Jiang, Y. Zhao, L. Zhu, S. Chen, X. Wang, Q. Wu, J. Ma, Y. Ma and Z. Hu, *Angew. Chem.,Int. Ed.*, 2011, **50**, 7132–7135.
21 C. H. Choi, S. H. Park and S. I. Woo, *Green Chem.*, 2011, **13**, 406–412.
22 S.-A. Wohlgemuth, R. J. White, M.-G. Willinger, M.-M. Titirici and M. Antonietti, *Green Chem.*, 2012, **14**, 1515–1523.
23 H. Jin, H. Zhang, H. Zhong and J. Zhang, *Energy Environ. Sci.*, 2011, **4**, 3389–3394.
24 D. H. Long, J. Zhang, J. H. Yang, Z. J. Hu, G. Cheng, X. M. Liu, R. Zhang, L. Zhan, W. M. Qiao and L. C. Ling, *Carbon*, 2008, **46**, 1259–1262.
25 G. C. Ruben and R. W. Pekala, *J. Non-Cryst. Solids*, 1995, **186**, 219–231.
26 M. M. Titirici and M. Antonietti, *Chem. Soc. Rev.*, 2010, **39**, 103–116.
27 R. J. White, M. Antonietti and M. M. Titirici, *J. Mater. Chem.*, 2009, **19**, 8645–8650.
28 R. J. White, N. Yoshizawa, M. Antonietti and M.-M. Titirici, *Green Chem.*, 2011, 2428–2434.
29 T.-P. Fellinger, R. J. White, M. M. Titirici and M. Antonietti, *Adv. Funct. Mater.*, 2012, **22**, 3254–3260.
30 V. K. Lamer and R. H. Dinegar, *J. Am. Chem. Soc.*, 1950, **72**, 4847–4854.

31 J. P. Paraknowitsch, A. Thomas and J. Schmidt, *Chem. Commun.*, 2011, **47**, 8283–8285.
32 Z. Li, N. Baccile, S. Gross, Z. Yuanjian, W. Wei, S. Yuhan, M. Antonietti and M. M. Titirici, *Carbon*, 2010, **48**, 3778–3787.
33 N. Baccile, M. Antonietti and M.-M. Titirici, *ChemSusChem*, 2010, **3**, 246–253.
34 M. Sevilla and A. B. Fuertes, *Chem.–Eur. J.*, 2009, **15**, 4195–4203.
35 M. Seredych, M. Khine and T. J. Bandosz, *ChemSusChem*, 2011, **4**, 139–147.
36 N. Baccile, G. Laurent, C. Coelho, F. Babonneau, L. Zhao and M.-M. Titirici, *J. Phys. Chem. C*, 2011, **115**, 8976–8982.
37 Z. Q. Li, C. J. Lu, Z. P. Xia, Y. Zhou and Z. Luo, *Carbon*, 2007, **45**, 1686–1695.
38 C. Vix-Guterl, E. Frackowiak, K. Jurewicz, M. Friebe, J. Parmentier and F. Beguin, *Carbon*, 2005, **43**, 1293–1302.
39 J. Zhang, *PEM fuel cell electrocatalysts and catalyst layers: fundamentals and applications*, Springer, 2008.
40 R. A. Sidik, A. B. Anderson, N. P. Subramanian, S. P. Kumaraguru and B. N. Popov, *J. Phys. Chem. B*, 2006, **110**, 1787–1793.
41 P. H. Matter, L. Zhang and U. S. Ozkan, *J. Catal.*, 2006, **239**, 83–96.
42 Z. Q. Luo, S. H. Lim, Z. Q. Tian, J. Z. Shang, L. F. Lai, B. MacDonald, C. Fu, Z. X. Shen, T. Yu and J. Y. Lin, *J. Mater. Chem.*, 2011, **21**, 8038–8044.
43 V. V. Strelko, V. S. Kuts and P. A. Thrower, *Carbon*, 2000, **38**, 1499–1503.